

Transport by Lagrangian Vortices in the Eastern Pacific

RYAN ABERNATHEY

Columbia University, New York, New York

GEORGE HALLER

ETH Zurich, Zurich, Switzerland

(Manuscript received 23 May 2017, in final form 18 January 2018)

ABSTRACT


Rotationally coherent Lagrangian vortices (RCLVs) are identified from satellite-derived surface geostrophic velocities in the eastern Pacific (180°–130°W) using the objective (frame invariant) finite-time Lagrangian coherent structure detection method of Haller et al. based on the Lagrangian-averaged vorticity deviation. RCLVs are identified for 30-, 90-, and 270-day intervals over the entire satellite dataset, beginning in 1993. In contrast to structures identified using Eulerian eddy-tracking methods, the RCLVs maintain material coherence over the specified time intervals, making them suitable for material transport estimates. Statistics of RCLVs are compared to statistics of eddies identified from sea surface height (SSH) by Chelton et al. RCLVs and SSH eddies are found to propagate westward at similar speeds at each latitude, consistent with the Rossby wave dispersion relation. However, RCLVs are uniformly smaller and shorter-lived than SSH eddies. A coherent eddy diffusivity is derived to quantify the contribution of RCLVs to meridional transport; it is found that RCLVs contribute less than 1% to net meridional dispersion and diffusion in this sector, implying that eddy transport of tracers is mostly due to incoherent motions, such as swirling and filamentation outside of the eddy cores, rather than coherent meridional translation of eddies themselves. These findings call into question prior estimates of coherent eddy transport based on Eulerian eddy identification methods.

1. Introduction

The mesoscale (broadly 10–500 km) is the most energetic scale in the ocean (Wortham and Wunsch 2014). Phenomenologically, the mesoscale comprises a disorderly jumble of waves, vortices, fronts, and filaments, and the word mesoscale frequently appears together with the word “eddy.” However, a survey of the literature reveals a wide range of definitions of “eddy,” which is used as both an adjective and a noun. The standard Eulerian statistical perspective defines “eddy” (an adjective) simply as a fluctuation about an Eulerian time and/or spatial mean state. The coherent structure perspective attempts to identify specific, discrete “eddies”

(a noun) and track them through the ocean. Here we seek to clarify the relationship between Eulerian eddy fluxes and coherent structures. Specifically, we seek to understand what fraction of the Eulerian eddy flux arises due to trapping and subsequent translation of water within material coherent structures.

Eulerian mesoscale eddy fluxes (i.e., statistical correlations between velocity and tracer fluctuations, also known as Reynolds fluxes) play a significant role in the transport of heat, salt, momentum, and other tracers through the ocean. Because climate models generally do not resolve the mesoscale, the subgrid-scale mesoscale flux must be parameterized based on the large-scale flow properties, commonly using a diffusive closure (Gent et al. 1995; Treguier et al. 1997; Visbeck et al. 1997; Vollmer and Eden 2013; Bachman and Fox-Kemper 2013). This important problem has motivated many studies of Eulerian eddy fluxes (and associated diffusivities) in observations and eddy-resolving models (e.g., Morrow et al. 1992; Stammer 1998; Roemmich and Gilson 2001; Jayne and Marotzke 2002; Volkov et al. 2008;

 Denotes content that is immediately available upon publication as open access.

Corresponding author: Ryan Abernathey, rpa@ldeo.columbia.edu

Fox-Kemper et al. 2013; Abernathey and Marshall 2013; Klocker and Abernathey 2014; Abernathey and Wortham 2015). This body of work has been largely unconcerned with coherent structures, although Abernathey and Wortham (2015) did note the overlap between eddy flux spectral characteristics and the lengths scales and propagation speeds of coherent mesoscale eddies.

Many different methods have been used to identify coherent structures (CSs). These methods fall into two general categories: Eulerian¹ (based on instantaneous features of the velocity field) and Lagrangian (based on time-dependent water parcel trajectories). Early Eulerian approaches used contours of the Okubo–Weiss (OW) parameter (Okubo 1970; Weiss 1991) to identify the boundaries of eddies (Isern-Fontanet et al. 2003, 2004). More recently, closed contours of the sea surface height (SSH) anomaly field have been employed (Chelton et al. 2011, hereinafter CSS11). The eddy census of CSS11 has been widely adopted by the community, likely due to its open publication on the web. Other recent Eulerian CS eddy census products include Dong et al. (2011) and Faghmous et al. (2015). While these methods differ in certain details, they are all fundamentally similar in that they use the instantaneous velocity field (or streamfunction) to identify eddies at each snapshot in time, and then track these features from one snapshot to the next.

This Eulerian approach to eddy tracking, however, suffers from several shortcomings [see Haller (2015) and Peacock et al. (2015) for discussions]. First, the structures identified in this way are not material; the Eulerian tracking algorithms associate spatially proximal features identified at neighboring time snapshots with a single object, but these features do not necessarily represent the same fluid. Second, the structures are not objective; different observers in frames translating and rotating relative to each other will identify different flow regions as coherent. This creates a conceptual problem because material transport by eddies should be independent of the observer, as required by basic axioms of continuum mechanics. A related issue is that OW and SSH eddies depend on arbitrary parameters or thresholds, which are routinely tuned to match expectations derived from the same methods. Finally, and most importantly from the perspective of transport, OW and SSHA eddies are materially incoherent to a significant extent; under Lagrangian advection, the supposed eddy boundaries become rapidly strained and filamented, implying that water leaks significantly across the structure boundaries

inferred by the OW and SSH criteria (Beron-Vera et al. 2013; Haller and Beron-Vera 2013).

Contradictions may therefore arise when such Eulerian eddy-tracking methods are applied to infer material transport, as in two recent studies. Dong et al. (2014) used Eulerian eddy tracking, together with vertical structure functions of potential temperature and salinity derived statistically from Argo profiles, to estimate the heat and salt content materially trapped inside the eddies. By assuming no exchange with the surrounding environment for the duration of the eddy lifetime, they estimated the meridional fluxes of heat and salt on a global scale, reaching the conclusion that “eddy heat and salt transports are mainly due to individual eddy movements.” Zhang et al. (2014) used a similar method to estimate the eddy mass flux. They employed tracked Eulerian eddies together with vertical structure functions to estimate the potential vorticity field surrounding the eddies. The outermost closed potential vorticity contour was assumed to constitute an impermeable material boundary for the duration of each tracked eddy, and the eddy motion was thereby translated to a mass flux. This method estimated the westward zonal eddy mass flux in the subtropical gyre regions to be approximately 30 Sv ($1 \text{ Sv} \equiv 10^6 \text{ m}^3 \text{ s}^{-1}$), a surprisingly large number that is comparable to the gyre transport itself. These approaches might seem quite appealing because they reduce the expensive problem of observing the turbulent ocean at high spatial and temporal frequency to the more tractable one of identifying and tracking a finite number of coherent eddies. However, the work of Beron-Vera et al. (2013), Haller and Beron-Vera (2013), and Wang et al. (2015) provides evidence that these methods strongly overestimate the degree of material coherence in mesoscale eddies, calling into question the findings.

The goal of the present study is to make a more accurate estimate of material transport due to ocean mesoscale eddies using an objective (i.e., frame independent) Lagrangian eddy detection method applied to surface velocity fields derived from satellite altimetry. We focus on a sector in the east Pacific that has been the setting for a number of studies on Eulerian eddy fluxes (Roemmich and Gilson 2001; Abernathey and Marshall 2013; Klocker and Abernathey 2014; Abernathey and Wortham 2015). We apply the recently introduced rotationally coherent Lagrangian vortex (RCLV) methodology based on a dynamic polar decomposition of the deformation gradient developed by (Haller 2016). The key difference between our approach and Eulerian eddy detection methods is that, by numerically advecting a dense mesh of millions of Lagrangian particles, we demonstrate (rather than assume) that our identified

¹ An Eulerian method for identifying coherent structures should not be confused with the Eulerian eddy flux.

vortices actually remain materially coherent throughout a finite time interval, as guaranteed by their mathematical construction. Furthermore, the full Lagrangian trajectories also allow us to estimate a more broadly defined material eddy flux due to the entire range of turbulent motions in the flow. By comparing this full flux with the transport due to the coherent vortices, we obtain an estimate of the relative importance of material transport by coherent structures to the full turbulent transport. We consider the two-dimensional surface geostrophic flow as observed by satellite altimetry, as this is the only large-scale velocity observation that resolves mesoscale structures, which limits our ability to probe subsurface transport. Our definition of transport by coherent vortices is strict: we only count water that is trapped and translated within the coherent eddy core and purposely exclude far-field effects such as stirring on the vortex periphery. Under this strict definition, we show that coherent transport accounts for only a small fraction of the total meridional eddy flux. Because of the possibility of the existence of a semicoherent periphery surrounding the coherent eddy core (Y. Wang et al. 2016), our estimates here might be considered a lower bound on this fraction.

The paper is organized as follows. In section 2, we review the RCLV definition and the concepts of Lagrangian dispersion and diffusivity. In section 3, we describe the satellite data and the numerical approach to Lagrangian particle advection. Section 4 provides some case studies of Lagrangian vortices identified by our algorithm and summarizes their statistics. In section 5, we present the eddy diffusivity and the coherent eddy diffusivity. Section 6 contains discussion and conclusions.

2. Theory of Lagrangian transport and rotationally coherent vortices

a. Eulerian eddy flux and Lagrangian diffusivity

Consider a conserved two-dimensional scalar $c(x, y, t)$ advected by a two-dimensional velocity field $\mathbf{u}(x, y, t)$ where $\mathbf{u} = (u, v)$. The time- and zonal-mean meridional flux of the scalar across a latitude circle in a sector of the ocean is given by \overline{vc} . The overbar represents the time and zonal average:

$$\overline{vc} = (L_x T)^{-1} \int_{x_0}^{x_0+L_x} \int_{t_0}^{t_0+T} vc \, dx, \quad (1)$$

where L_x is the zonal extent of the sector and T is the averaging time period. We observe that \overline{vc} , as any scalar flux across a designated surface, is objective, that is, independent of the observer (see appendix for proof of

objectivity). To capture the contribution of eddies to the mean meridional flux accurately, one therefore needs an observer-independent eddy-identification scheme.

The Lagrangian dynamics of the flow are described by the kinematic equation

$$\frac{\partial \mathbf{X}}{\partial t} = \mathbf{u}, \quad (2)$$

where $\mathbf{X} = (X, Y)$ is the position vector. We denote the initial fluid parcel positions at $t = 0$ as $\mathbf{x}_0 = (x_0, y_0)$. We can use this initial position to label the fluid parcels at a later time: $\mathbf{X} = \mathbf{X}(x_0, y_0, t)$. For homogeneous, statistically stationary turbulent flow, Taylor (1921) identified the relationship between the Eulerian mean flux \overline{vc} and the Lagrangian statistics as

$$\overline{vc} = -K_{\text{abs}} \frac{\partial \overline{c}}{\partial y} \quad (3)$$

with

$$K_{\text{abs}} = \frac{1}{2} \frac{\partial}{\partial t} \overline{(\Delta Y)^2}. \quad (4)$$

where $\Delta Y = Y - y_0$ is the displacement of a water parcel from its initial position; $\overline{(\Delta Y)^2}$ represents the mean squared displacement, that is, absolute dispersion; and K , the growth rate of this absolute dispersion, represents the single particle or absolute diffusivity (Taylor 1921; LaCasce 2008). Regardless of whether the flow statistics are truly diffusive or not, (3) and (4) represent the kinematic relationship between Lagrangian displacement and Eulerian flux. The diffusivity K_{abs} expresses the fundamental transport properties of the flow, independently of the background gradient $\partial \overline{c} / \partial y$. As shown in the appendix, K_{abs} is objective, that is, it is invariant under a change in observer reference frame (including Galilean transforms), provided that the distance between the particle and its initial position is measured in the observer's current reference frame. Subtle differences in definition might explain why previous authors have claimed that K_{abs} is not Galilean invariant (LaCasce 2008). The definition used here is the one most relevant for material transport.

From an Eulerian perspective, the eddy component of the flux is readily identified via a standard Eulerian Reynolds decomposition: $\overline{vc} = \overline{v} \overline{c} + \overline{v'c'}$, where the prime indicates the instantaneous deviation from the Eulerian mean. The second term $\overline{v'c'}$ is commonly termed the eddy flux. Taylor envisioned a homogeneous, isotropic turbulent flow with no mean component, that is, $\overline{v} = 0$, such that $\overline{vc} = \overline{v'c'}$. In contrast, most geophysical flows have mean flows, and the mean

advection can influence K_{abs} . One way to remove the effects of the mean flow in the Lagrangian frame is to instead focus on the relative diffusivity (Batchelor 1952; Bennett 1984):

$$K_{\text{rel}} = \frac{1}{2} \frac{\partial}{\partial t} \overline{(Y - \bar{Y})^2}, \quad (5)$$

which represents the growth rate of the second moment of the ensemble displacement. In this case, the ensemble consists of all water parcels originating at a particular latitude. [Relative diffusivity can equivalently be calculated from pair separation statistics (LaCasce 2008). Also note that K_{rel} is unchanged if ΔY is used in place of Y , since $\bar{y}_0 = y_0$.] A detailed discussion of the relationship among K_{abs} , K_{rel} , and the mixing of a passive tracer is given by Klocker et al. (2012). For the purposes of this study, we shall take K_{rel} to be the most relevant diagnostic of net meridional eddy transport in our sector. Our goal is to identify the contribution of coherent Lagrangian eddies to K_{rel} . Like K_{abs} , K_{rel} is an objective quantity (see appendix). As noted above, a self-consistent and accurate assessment of the coherent-eddy component K_{rel} should also be based on objective eddy identification schemes, such as the one described next.

b. Rotationally coherent Lagrangian vortices

To partition the transport defined in (4) and (5) into a contribution from coherent Lagrangian eddies, the domain must be divided into regions inside and outside a suitably defined eddy boundary. For the boundary to be relevant for transport it must be a material line (in 2D) or surface (in 3D) derived from an objective (frame invariant) method. The identification of such boundaries in unsteady turbulent flows is the subject of much recent work from the field of dynamical systems, and several possible criteria exist [for a review, see Haller (2015)]. We emphasize again that the Eulerian eddy identification methods of CSS11 are not objective and depend on choices of thresholds and parameters. Consequently, they yield boundaries that, when advected as material lines, rapidly deform and disperse away from the supposed eddy center (Beron-Vera et al. 2013; Haller and Beron-Vera 2013).

One sensible criterion is to define eddy boundaries as closed material curves that experience minimal tangential stretching over a finite-time interval, so-called elliptic Lagrangian coherent structures (LCSs; Haller and Beron-Vera 2012). A more general approach locates material eddy boundaries that exhibit uniform stretching and hence show no filamentation (Haller and Beron-Vera 2013). The elliptic LCS detection methods have been applied to study Agulhas rings (Beron-Vera

et al. 2013; Haller and Beron-Vera 2013; Wang et al. 2015). The underlying variational principles guarantee perfect lack of filamentation for the boundaries and hence tend to be stringent and computationally complex. [Recent work by Serra and Haller (2017) has, however, simplified the necessary computations considerably.]

Here we opt for a fluid-mechanically more intuitive approach based on vorticity. Building on the initial ideas of Farazmand and Haller (2016), Haller et al. (2016) showed that RCLV boundaries can be identified as the outermost closed contours of the Lagrangian-averaged vorticity deviation (LAVD, defined below). The physical essence of an RCLV is the notion that all fluid parcels along a coherent material vortex boundary should rotate at the same average angular velocity over a finite-time interval, in analogy to solid body rotation. The LAVD technique enables the identification of such coherently rotating structure boundaries from Lagrangian trajectory data. Haller et al. (2016) further showed that the RCLVs identified in this way coincided with structures identified by the earlier elliptic LCS methods, although the RCLV boundaries were larger.² Given the relative computational simplicity and the familiarity of vorticity to most physical oceanographers, we adopt this approach as our eddy identification technique. Here we briefly review the practical elements of the theory and refer the reader to Haller et al. (2016) for a deeper mathematical treatment.

The instantaneous relative vorticity in two dimensions is

$$\zeta(x, y, t) = -\frac{\partial u}{\partial y} + \frac{\partial v}{\partial x}. \quad (6)$$

The vorticity deviation is obtained by subtracting the spatial average, that is, $\zeta'(x, y, t) = \zeta - \langle \zeta \rangle(t)$. (Angle brackets indicate an average over the whole computational domain.) Subtracting the mean vorticity field removes any solid body rotation of the entire domain and is required to maintain the frame invariance of the method (Haller et al. 2016). In practice, however, when the domain is the entire ocean, the mean vorticity is rather negligible. A Lagrangian-averaged quantity is the instantaneous quantity averaged along the evolving flow trajectory (as opposed to an Eulerian average at a fixed location). The LAVD is hence given by

²These larger boundaries are no longer guaranteed to be completely free from filamentation under material advection. However, by construction, any filamentation they might exhibit is tangential to the boundary, and hence the stretched boundary keeps traveling with the eddy without global breakaway.

$$\text{LAVD}_{t_0}^{t_1}(x_0, y_0) = \frac{1}{t_1 - t_0} \int_{t_0}^{t_1} |\zeta'[X(x_0, y_0, t), Y(x_0, y_0, t), t]| dt. \quad (7)$$

The LAVD is a function of position (x_0, y_0) but also depends on the time interval t_0, t_1 . RCLV boundaries at time t_0 are then defined as the outermost convex and closed LAVD curves surrounding local maxima of the LAVD field. The maxima themselves are the Lagrangian vortex centers, which can be proven to be attractors or repellers for floating debris, depending on the polarity of the eddy (cf. Haller et al. 2016). Details of the numerical computation of RCLVs are given in section 4.

Once the RCLVs are identified for a specific time interval, it is straightforward to compute the associated contribution to dispersion and diffusivity. We define a masking function $m_{t_0}^{t_1}$ to be 1 inside each RCLV boundary and 0 outside. The *coherent relative diffusivity* is then defined as

$$K_{\text{rel}}^{\text{cs}} = \frac{1}{2} \frac{\partial}{\partial t} \overline{m_{t_0}^{t_1} (Y - \bar{Y})^2}. \quad (8)$$

The $m_{t_0}^{t_1}$ factor masks all regions that are not within a coherent structure, effectively assuming such regions move only with the mean flow and induce no relative dispersion. [Note that, regardless of the masking factor, \bar{Y} in (8) and (5) is the same; the displacement is always relative to the mean displacement of the full ensemble of particles deployed at latitude y_0 .] By comparing $K_{\text{rel}}^{\text{cs}}$ with K_{rel} , we thereby quantify the fraction of meridional eddy transport due to coherent structures. If it is true that eddy transport is “mainly due to individual eddy movements” (Dong et al. 2014), then $K_{\text{rel}}^{\text{cs}} \simeq K_{\text{rel}}$. In contrast, if most of the transport is due to *incoherent* motion outside of the structures, then $K_{\text{rel}}^{\text{cs}} \ll K_{\text{rel}}$. Note that $K_{\text{rel}}^{\text{cs}}$ includes two distinct modes of dispersion: coherent meridional motion of the whole eddy and rotation of the water within the eddy. Because of the strict separation of the domain into *inside* and *outside*, we exclude any possible far-field effects of the eddies on transport, including partial entrainment of water into the semicoherent eddy periphery [a scenario described by Y. Wang et al. (2016)] as well as the more general long-range influence of vorticity anomalies on the global flow field (as suggested by the potential vorticity inversion principle). Our aim in (8) is not to account for every possible way in which coherent eddies influence transport but simply to measure the fraction of transport due to trapping and translation of the coherent core. Consequently, (8) may represent a lower bound on the overall contribution of such structures to transport.

The coherent diffusivity $K_{\text{rel}}^{\text{cs}}$ defined in (8) can only be calculated for material eddies, such as those identified from objective LCS methods. For nonmaterial eddies, such as those identified from tracked Eulerian SSH contours (CSS11) or potential-vorticity contours (Zhang et al. 2014), the position of the tracked eddy itself generally diverges from the Lagrangian trajectories of particles contained within the boundary at t_0 . This renders (8) ambiguous: should one follow the actual particles or the tracked eddy boundaries? For this reason, we do not attempt to provide an estimate of $K_{\text{rel}}^{\text{cs}}$ for Eulerian eddy datasets. We also note that the dispersion statistics of Eulerian vortices have already been studied in some detail (Hansen et al. 1998; LaCasce 2008) and may be related to $K_{\text{rel}}^{\text{cs}}$.

3. Satellite data and particle advection

To identify RCLVs and compute relative dispersion, we use satellite-derived surface geostrophic velocities to numerically advect virtual Lagrangian particles. In this study, we consider only transport by the two-dimensional near-surface geostrophic velocity. This is, of course, an incomplete representation of the full flow field, but the geostrophic flow is by far the dominant component at the scales of interest here. It was shown by Rypina et al. (2012) that Ekman currents, the main large-scale ageostrophic motion in the open ocean, make a negligible contribution to mesoscale dispersion compared to the geostrophic flow. In the conclusions, we speculate about the possible role of ageostrophic and/or unresolved motion for the detection of RCLVs.

a. AVISO surface geostrophic velocities

The surface geostrophic velocity field \mathbf{v}_g is related to the SSH relative to the geoid η via

$$\hat{\mathbf{k}} \times \mathbf{v}_g = -\frac{g}{f} \nabla \eta, \quad (9)$$

where f is the Coriolis parameter, g is the gravitational acceleration, and $\hat{\mathbf{k}}$ is the unit vector pointing out of the sea surface. Satellite altimetry measures the SSH η .

We employ precomputed gridded geostrophic velocities from AVISO. The altimeter products were produced by SSALTO/Developing Use of Altimetry for Climate Studies (DUACS) and distributed by AVISO, with support from CNES (<http://www.aviso.altimetry.fr/duacs/>). The AVISO gridding process uses objective interpolation (Barnes 1964;

their terminology is unrelated to the objectivity of coherent structures) to map along-track satellite radar altimetry from various platforms onto a $1/4^\circ$ latitude–longitude grid (Ducet et al. 2000). In addition to providing precomputed geostrophic velocities, this product also applies a higher-order vorticity balance to estimate velocities in the equatorial region (within $\pm 5^\circ$) where geostrophy does not hold (Lagerloef et al. 1999). While this provides a complete global surface velocity field, the results in this equatorial band are less reliable. The data were downloaded in 2015 and reflect the most recent AVISO algorithm and processing available at that time. We use the delayed-time, reference, all-satellite merged product. We consider the time period from 1 January 1993 to 17 October 2014.

An additional processing step was undertaken: we applied a small correction to the AVISO geostrophic velocity field to remove the divergence due to the meridional variation of f and to enforce no-normal-flow boundary conditions at the coastlines. The resulting velocity field, henceforth denoted simply \mathbf{v} , is an exactly two-dimensional nondivergent flow. The correction procedure is described in detail by Abernathey and Marshall (2013), who demonstrate that the corrections are small in magnitude compared to the original geostrophic velocity. We compared corrected versus noncorrected LAVD fields and found a negligible impact on the identification of RCLVs in the open ocean.

b. Advection of Lagrangian particles

As noted by Haller et al. (2016), the LAVD field may contain structure on smaller scales than the scales of the velocity field itself. This is related to the fact that a relatively coarse chaotic advection field can produce very fine structure in passive tracers (Pierrehumbert 1991). Practically, it means that an extremely dense mesh of Lagrangian particles is required to properly resolve the LAVD. This leads to a significant computational burden if, as here, one wishes to study a large geographical area and temporal extent. The AVISO product is gridded at $1/4^\circ$ resolution and resolves SSH anomalies of roughly 50 km and larger (CSS11). However, sensitivity tests indicated that an initial particle spacing of $1/32^\circ$ is necessary to achieve sufficient accuracy in the LAVD field and identification of RCLVs. The mesh of initial positions is located between 180° and 130°W longitude and 80°S and 80°N latitude, a total of 8 192 000 points. (In retrospect, many of the high-latitude particles were not useful, since they lie within land points or within the marginal sea ice zone where AVISO velocities are not available. We restrict the analysis to the latitude range 65°S – 60°N .)

The initial particle positions (at time t_0) determine the discrete coordinates of the LAVD field. These initial positions can therefore be chosen to facilitate the

identification of RCLVs. In particular, the first step in the algorithm requires the maxima of LAVD to be identified (Haller et al. 2016). The most obvious initial deployment, a rectangular grid, is actually not ideal for the robust identification of maxima because the relationship between diagonally connected points is ambiguous; a better choice is a hexagonal grid, in which each point has six unambiguous neighbors (Kuijper 2004). To transform a rectangular mesh to a hexagonal one, every other row is offset by $\Delta x/2$, where $\Delta x = 1/32^\circ$ is the spacing in the zonal direction.

We seek to identify RCLVs with lifetimes of 30, 90, and 270 days. Accordingly, we segment the time domain into nonoverlapping N -day intervals (265 intervals for 30-day periods, 88 intervals for 90-day periods, and 29 intervals for 270-day periods). While the specific interval bounds are arbitrary, RCLVs are structurally stable by construction, that is, small changes in the extraction interval will have a small effect. If we identify an RCLV over a given time interval, this structure will generally be a subset of a larger RCLV that we would obtain in the same location for shorter time intervals. Thus, we would not lose any of the RCLVs if we picked shorter time intervals (unless we pick such short intervals that Lagrangian coherence can no longer be established from the available data). Rotational coherence is a finite-time notion, and hence the same water mass may become incoherent over longer times. It is still possible that we miss some short-lived RCLVs over longer time intervals.

The Lagrangian trajectories are determined by solving the equation $d\mathbf{X}/dt = \mathbf{v}$ numerically using the MITgcm (Adcroft et al. 2018), an ocean general circulation model. Although this model is primarily designed for prognostic ocean simulations, it has several features that make it an attractive choice for computationally demanding Lagrangian simulations. First, it can operate in offline mode, in which velocity fields are read from files. Second, it supports Lagrangian particle tracking (via the flt package) and implements fourth-order Runge–Kutta integration. Finally, MITgcm can run efficiently in a massively parallel configuration on many nodes of a high-performance computing cluster, providing the necessary memory and CPU performance to enable large Lagrangian ensembles.

An MITgcm run was performed for each of the temporal segments described above, and particle data were output daily. (Relative vorticity was calculated on the Eulerian grid and interpolated bilinearly to particle positions.) The total data volume of output generated for the study was over 2 TB. The identification of RCLVs from these data is described in the following section.

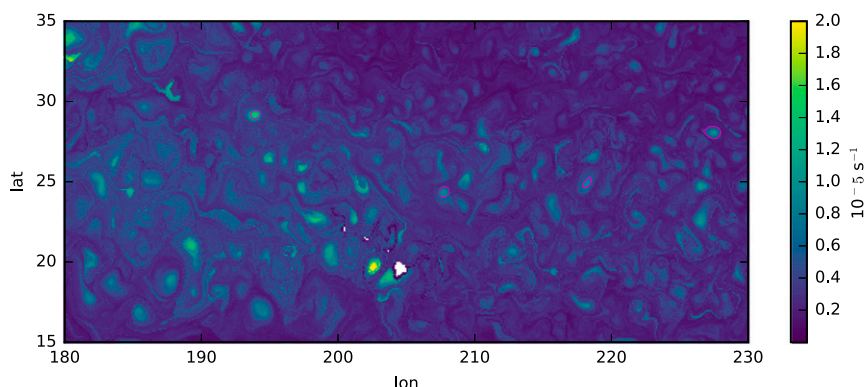


FIG. 1. A close-up example of a 90-day LAVD field from the region near Hawaii. Identified RCLV boundaries are shown as magenta contours. Note that the large local LAVD maximum just west of Hawaii is not associated with an RCLV because the LAVD field near the maximum exhibits a spiraling filamentary structure. (This is indicative of vortex breakup during the interval.).

4. Identification and statistics of Lagrangian vortices

a. Algorithm

The algorithm employed for identifying RCLVs follows Haller et al. (2016), with some slight modifications for computational efficiency.

- 1) At time t_0 , initialize a hexagonal mesh of Lagrangian particles over the domain.
- 2) Advect particles forward until time $t_0 + T$, where T is the desired vortex lifetime (here 30, 90, and 270 days). Output particle position and relative vorticity every day.
- 3) Average the vorticity deviation (absolute value of relative vorticity minus global mean vorticity) over particle trajectories and map back to initial positions \mathbf{x}_0 . The resulting field is the LAVD.
- 4) Identify maxima of LAVD. (Maxima are unambiguously identified on a hexagonal mesh.) These are the RCLV centers.
- 5) Find the largest closed and convex curves around LAVD maxima. These are the RCLV boundaries. The regions are grown iteratively by adding points; iteration stops when the next point to be added lies within the convex hull of the current region. This method admits a small convexity deficiency (usually of order 0.01) in the curves to account for the discrete nature of the numerically computed LAVD field.
- 6) Filter the RCLVs by discarding features with area below a minimal admissible size (here chosen to be the area of a circle with a diameter of 30 km).

This algorithm, as well as other general-purpose data processing routines for MITgcm particle trajectories, was implemented in a Python package called floater (available at <https://github.com/rabernat/floater>). An

example of the LAVD field, together with the positions of identified RCLVs, is shown in Fig. 1.

b. Example vortices

The initial and final locations of two randomly selected 90-day RCLVs are shown in Fig. 2, superimposed on the SSH anomaly field. One is located in the North Pacific subtropical gyre, while the other is in the Antarctic Circumpolar Current. These vortices clearly remain materially coherent over the 90-day lifetime, consistent with the results of (Haller et al. 2016). We examined hundreds of examples and found similar behavior. This should be contrasted to the behavior of SSH eddies, whose boundaries are rapidly deformed under advection by the surface geostrophic flow (Beron-Vera et al. 2013).

One noteworthy feature of these example RCLVs is that they do appear embedded within SSH anomalies. However, the coherent core is much smaller than the SSH anomaly. Here we do not attempt to comprehensively compare the RCLVs with tracked SSH eddies on a feature-by-feature basis, but a statistical comparison (next subsection) suggests that this difference in size holds in general.

c. Vortex statistics

In this section, we calculate some statistics of all the identified RCLVs and compare them to the statistics of the tracked SSH eddies of CSS11, whose data are publicly available (<http://wombat.coas.oregonstate.edu/eddies/>). We identified 41 875 RCLVs for the 30-day intervals, 1182 RCLVs for the 90-day intervals, and only 1 RCLV for the 270-day intervals in the period 1993–2015. The trajectories for all the 30-day RCLVs are plotted in Fig. 3. The average number of RCLVs per degree of latitude per year is plotted in Fig. 4. (270-day RCLVs are excluded

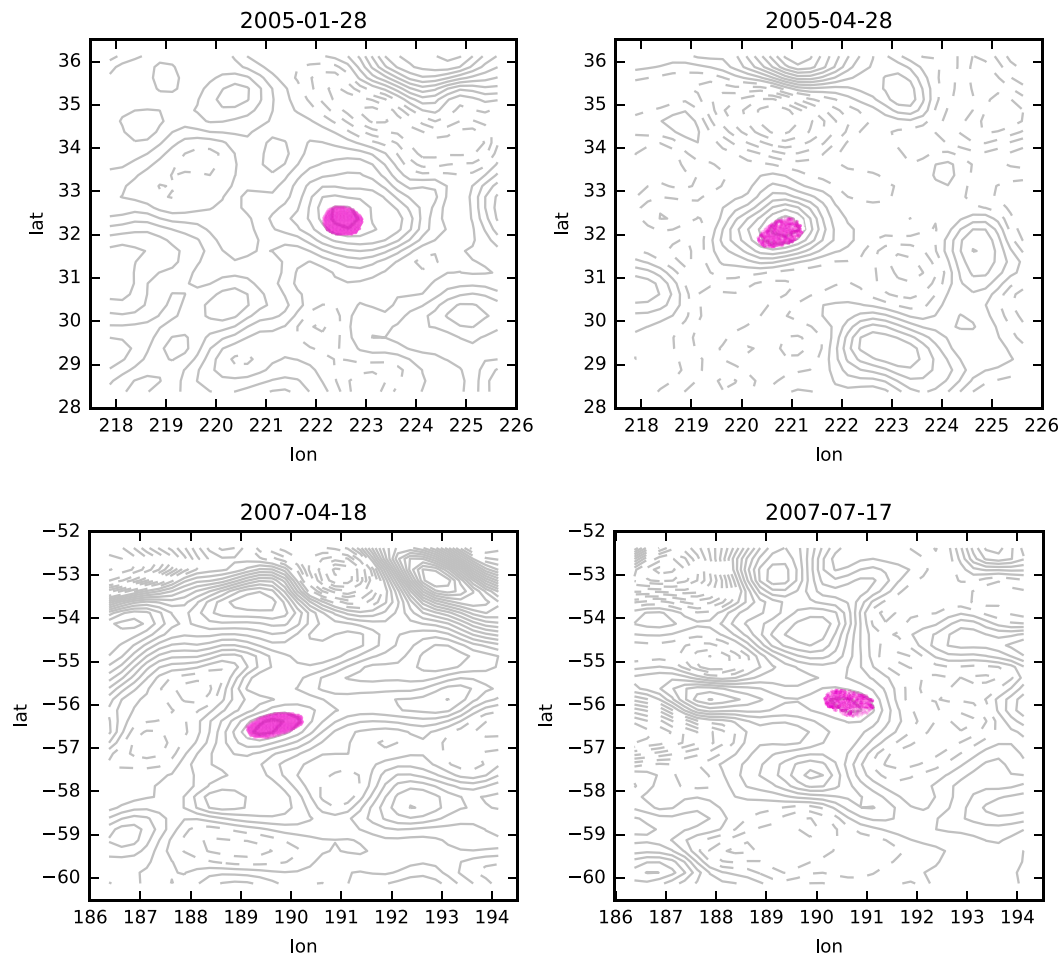


FIG. 2. The (left) initial and (right) final locations of two randomly selected 90-day RCLVs in the (top) northern and (bottom) southern hemispheres. The points contained within each RCLV boundary are visualized as magenta dots, overlaid on the contours of SSH anomaly. The contour interval for SSH is 2 cm.

from all subsequent discussion, since they are almost nonexistent.) Both figures reveal the densest concentration of RCLVs in midlatitudes, with very few RCLVs detected in the tropics. This is broadly similar to SSH eddies.

The comparison of the occurrence of 30-day versus 90-day RCLVs in Fig. 4 reveals that the shorter-lived vortices are much more prevalent. There are actually more 30-day RCLVs than SSH eddies with lifetimes larger than 30 days. However, the reverse is true for 90-day RCLVs; there are many more SSH eddies with equivalent or longer lifetimes. The comparison with 270-day RCLVs, which are essentially nonexistent, is even more extreme; the census of CSS11 identifies 2076 SSH eddies with lifetimes at least that long.

We now examine the statistics of eddy size. The RCLV horizontal area A_{xy} is converted to a radius r via the formula $r = \sqrt{A_{xy}/\pi}$. Most of the RCLVs are approximately circular (e.g., Fig. 2), and this conversion yields a familiar unit for assessing length scales. In Fig. 5, we plot this

radius and compare it to the radius of SSH eddies from CSS11. Statistics are calculated in 5° latitude bins.

Outside of the tropics (where RCLVs are rare), Fig. 5 reveals a familiar inverse relationship between eddy size and latitude, which likely reflects the dependence of the Rossby deformation radius on the Coriolis parameter (Chelton et al. 1998). The largest median RCLV radius occurs near $\pm 30^\circ$, where it approaches 40 km. Comparing with CSS11, the median RCLV radius is roughly about half of the median SSH eddy. This is consistent with the example vortices shown in Fig. 2. The SSH size statistics diverge qualitatively from the RCLVs in the tropics.

In Fig. 6, we examine the zonal propagation speed c_x of RCLVs and SSH eddies. In both cases, the zonal propagation speed is calculated as the total zonal distance traveled over the eddy lifetime. From this point of view, RCLVs and SSH eddies look very similar, with much faster propagation at low latitudes due to the larger gradient in Coriolis parameter (i.e., β effect;

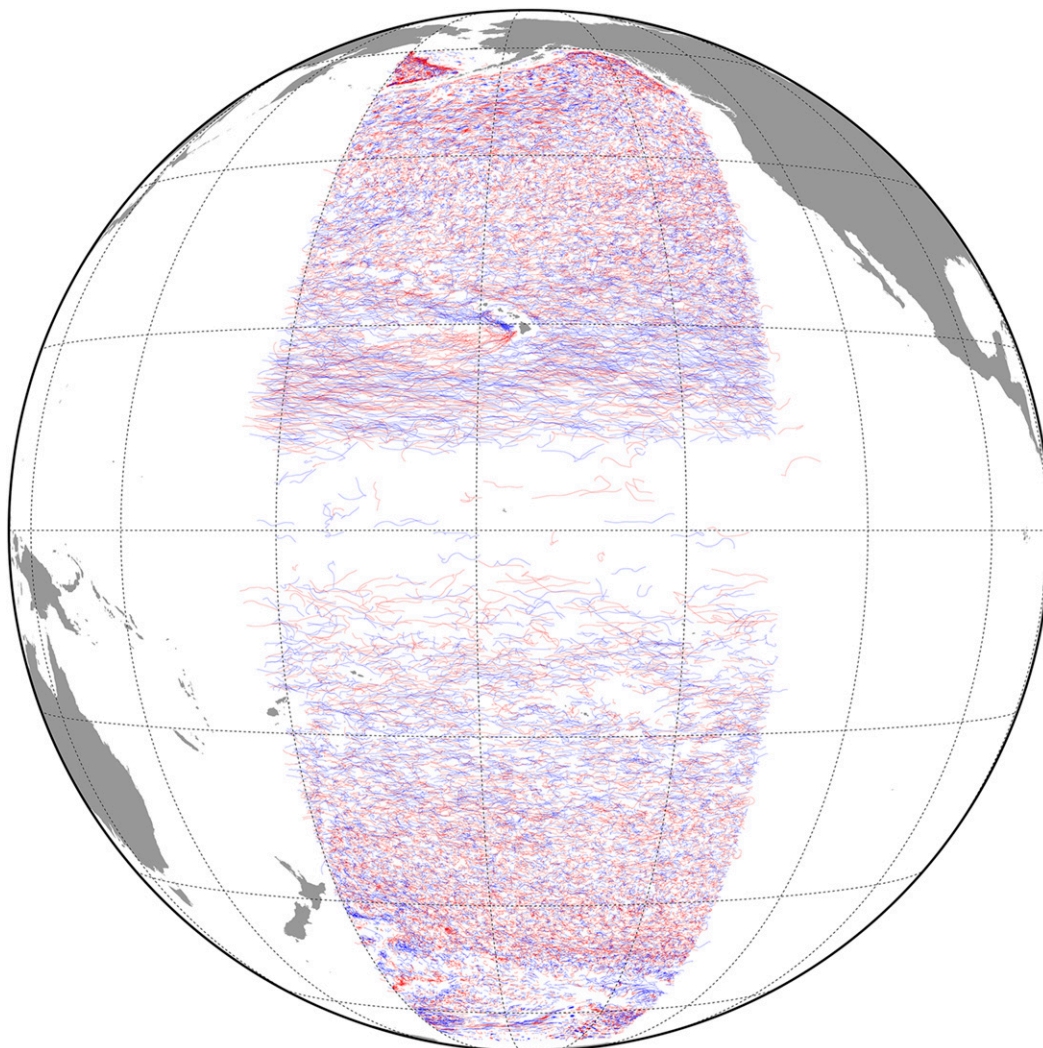


FIG. 3. The trajectories of the center points of all 46 486 thirty-day RCLVs identified in the period 1993–2015. Trajectories represent actual Lagrangian water parcel paths under advection by the surface geostrophic flow. Cyclonic vortices are shown in blue and anticyclonic are shown in red.

CSS11; Klocker and Abernathey 2014; Abernathey and Wortham 2015). Again, the statistics diverge in the tropics, where there are vanishingly few RCLVs.

Since the RCLVs and SSH eddies propagate at the same speed, one might expect that the Eulerian methods of CSS11 and the Lagrangian method used here identify broadly similar structures. However, the radius statistics suggest that the rotationally coherent core of mesoscale eddies is considerably smaller (by half) than the radius inferred by CSS11. Furthermore, there is a significant difference in eddy lifetime; the SSH eddies last much longer than the RCLVs. This might indicate that many SSH eddies represent materially leaky dynamical structures, which exchange water with their surroundings. While we have not conducted a comprehensive investigation of RCLV lifetime, the fact that there were essentially zero 270-day RCLVs in the sector provides an

upper bound for the time scale of this leaky exchange. On the other hand, Wang et al. (2015) found numerous materially coherent Agulhas eddies with 360-day lifetimes, suggesting that different regions of the ocean may generate less leaky eddies. This discrepancy may be addressed in future work by applying the RCLV method at a global scale.

5. Transport by Lagrangian vortices

Having described the method of identifying coherent Lagrangian vortices, we now turn to the central question of our study: the role of these RCLVs in material transport.

a. Advective transport

First, we address the question of advective volume transport by the RCLVs. By combining radius and zonal

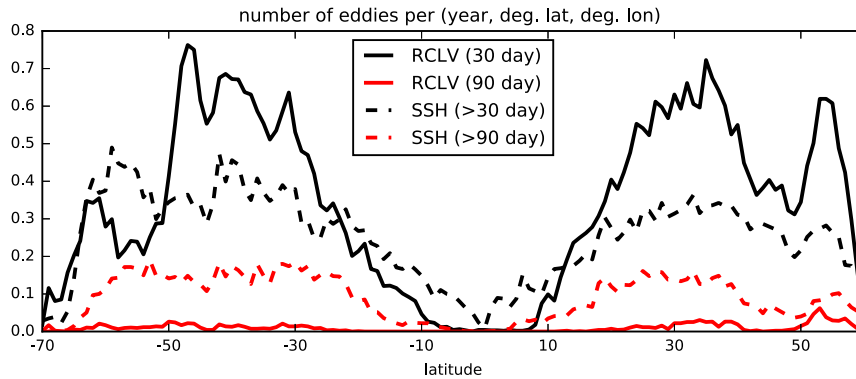


FIG. 4. Number of eddies per year per square degree of latitude/longitude in the east Pacific sector for RCLVs (this study; solid line) and SSH eddies (CSS11; dashed line). The colors correspond to the eddy lifetime; black shows lifetimes of ≥ 30 days and red shows lifetimes of ≥ 90 days.

propagation and assuming a vertical depth scale, we can arrive at an estimate of the advective volume transport by the RCLVs that is directly comparable with Zhang et al. (2014). First, we define the approximate cross-sectional area of each RCLV in the latitude–depth plane as $A_{yz} = 2rh$, where h is a representative depth scale of the RCLV in the vertical. In reality, each RCLV will have its own

unique depth profile, which is likely strongly dependent on latitude and stratification. However, the satellite data give us no information about the depth dependence of the flow, so we make an extremely crude assumption: we just take $h = \text{const} = 500$ m for all eddies. The scale depth of 500 m was chosen based on the findings of Roemmich and Gilson (2001), who analyzed the depth

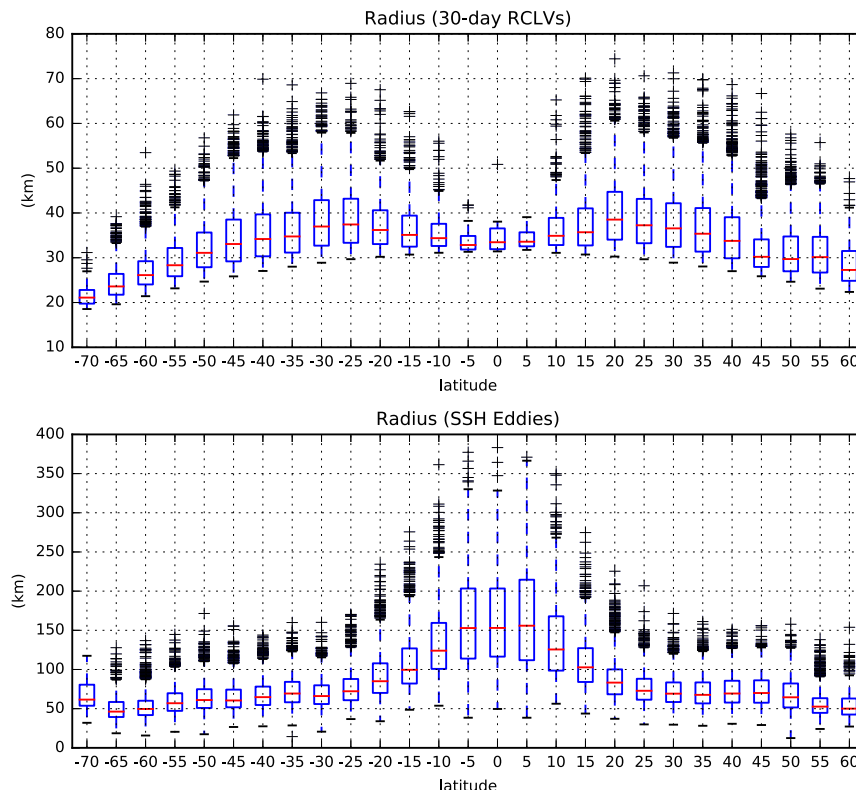


FIG. 5. Radius statistics of (top) 30-day RCLVs and (bottom) all SSH eddies. Statistics of all eddies in 5° bins are shown using a box-and-whisker plot. The red line indicates the median. The blue box spans the middle two quartiles (25th–75th percentiles) of the distribution. The black whiskers span the 10th–90th percentiles. Outliers are shown using the black + symbol.

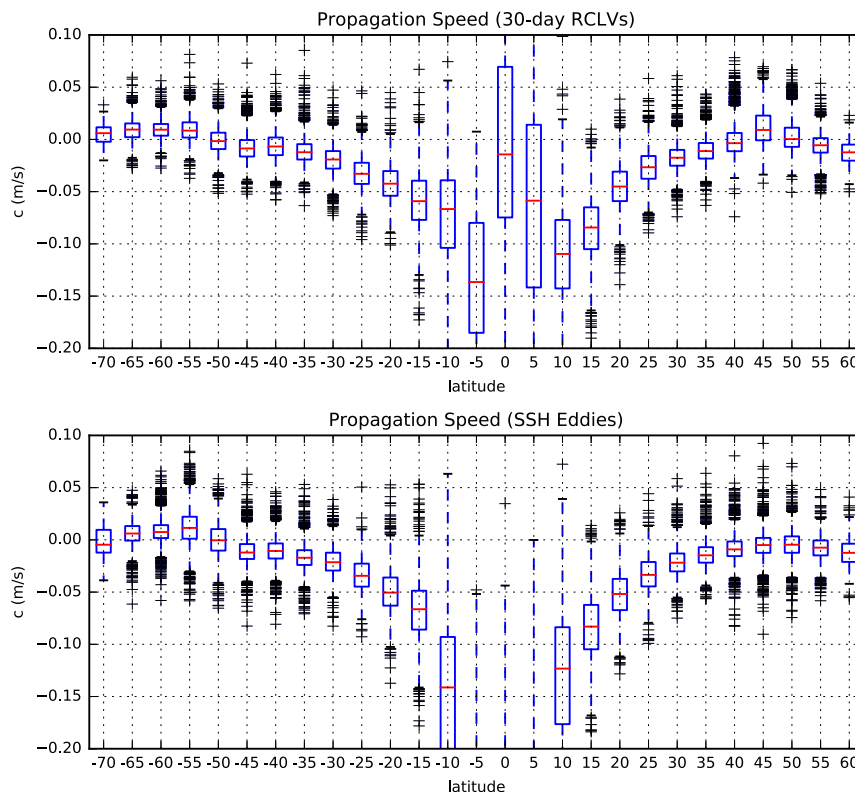


FIG. 6. As in Fig. 5, but for eddy zonal propagation speed.

dependence of mesoscale temperature anomalies in this sector. We consider the resulting transport estimate to be accurate only within an order of magnitude.

Following Wang et al. (2015), we identify all RCLVs crossing specific longitude lines (170° , 160° , 150° , and 140° W) over their 30- and 90-day lifetimes. The instantaneous zonal transport of each individual RCLV is given by $c_x A_{yz}$. We sum the individual contributions in 5° bins and then time average over the whole 25-yr study period. The results of this calculation are shown in Fig. 7. The peak value of the zonal transport for 30-day RCLVs is between -0.1 and -0.2 Sv per degree latitude, with a net meridionally integrated transport of approximately 3 Sv across the whole sector. The standard deviation (error bars in Fig. 7) is much greater than the mean, indicating the intermittent nature of the zonal transport. For comparison, in this sector Zhang et al. (2014) obtained peak values of around -0.5 Sv per degree latitude, with a net transport of around 30 Sv (their Fig. 3). Notwithstanding the uncertainty due to our use of a constant depth scale, it is clear that our 30-day RCLVs are associated with considerably less zonal transport than that estimated by Zhang et al. (2014). For the 90-day RCLVs, the estimated zonal transport is an order of magnitude lower.

We also compute the meridional advective transport across latitude circles. The results, shown in Fig. 8, reveal that the mean meridional advective transport is extremely small compared to its standard deviation. (The standard deviation is related to the meridional dispersion examined in the next subsection.) Nevertheless, in the mean of the 30-day RCLVs, a similar pattern to Zhang et al. (2014) is discernible, with northward transport throughout the South Pacific and tropical North Pacific and southward transport in the mid-latitude North Pacific. The transport values again are roughly an order of magnitude less than those of Zhang et al. (2014). For both meridional and zonal advective transport, the magnitude appears to be highly dependent on the eddy lifetime.

b. Meridional dispersion and diffusion

Now we examine the dispersion and diffusion associated with the RCLVs, which is the diagnostic most relevant to tracer transport. For each 30- and 90-day interval, we compute the absolute diffusivity K [(4)] and relative diffusivity K_{rel} [(5)] as a function of latitude using the full ensemble of Lagrangian particles. We also compute the fractional relative diffusivity $K_{\text{rel}}^{\text{cs}}$ [(8)], using only particles inside the RCLVs. As discussed in

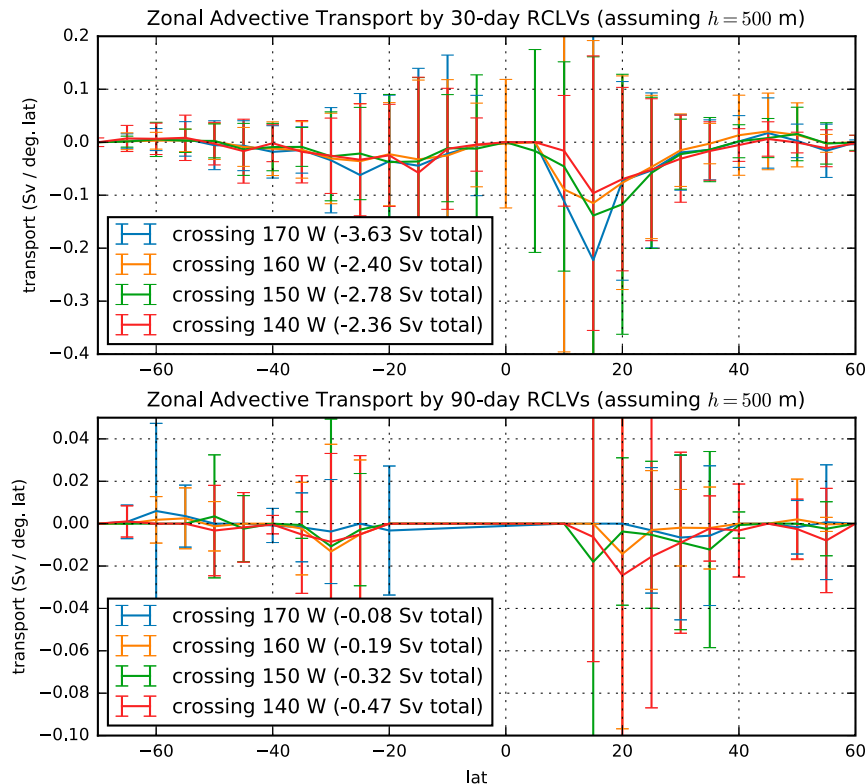


FIG. 7. Zonal advective transport across four different longitude lines for the RCLVs, calculated assuming a depth scale of 500 m. The error bar indicates one standard deviation of the time average over all time windows (30 days and 90 days).

section 2, $K_{\text{rel}}^{\text{cs}}$ represents the diffusivity that would result if water parcels outside of the RCLVs moved only with the zonal-mean flow and induced no relative dispersion.

The results of these diffusivity calculations are shown in Fig. 9. First, we note that there is minimal difference between K and K_{rel} , revealing that there is negligible mean meridional advection throughout the sector. The value of K_{rel} ranges from 500 to 6000 $\text{m}^2 \text{s}^{-1}$, with highest values found in the tropics. This is broadly consistent with previous estimates from this sector (Zhurbas and Oh 2003; Abernathey and Marshall 2013; Klocker and Abernathey 2014; Abernathey and Wortham 2015). Precise agreement with previous studies is not necessarily expected, since relative diffusivity depends sensitively on the time interval (Okubo 1971; Ollitrault et al. 2005; LaCasce 2008). For homogeneous flows, convergence is expected for long time scales (Klocker et al. 2012), but the diffusivities here correspond precisely to 30- and 90-day time intervals. The difference between the 30- and 90-day results show that convergence has not been reached everywhere.

The emphasis here is not the precise value of K_{rel} but rather the comparison with $K_{\text{rel}}^{\text{cs}}$ (Fig. 9, middle). The most striking difference is the order of magnitude: $K_{\text{rel}}^{\text{cs}}$

does not exceed $10 \text{ m}^2 \text{s}^{-1}$ for 30-day RCLVs and does not exceed $1 \text{ m}^2 \text{s}^{-1}$ for 90-day RCLVs. We can quantify the fraction of transport accomplished by RCLVs at each latitude via the ratio $R_K = K_{\text{rel}}^{\text{cs}}/K_{\text{rel}}$, as plotted in Fig. 9 (bottom). This fraction would be close to one if most of the transport was by coherent vortices; instead, we observe that it never exceeds 0.005 for 30-day RCLVs and is an order of magnitude smaller for 90-day RCLVs. This small contribution of RCLVs to the meridional transport mirrors the finding of Wang et al. (2015) that materially coherent Agulhas eddies make a very small contribution to net transport in that region—we return to this point in section 6.

The similarity between the shape of $K_{\text{rel}}^{\text{cs}}$ and the average density of RCLVs (Fig. 4) suggests that the primary control on $K_{\text{rel}}^{\text{cs}}$ is simply the density of RCLVs found at a particular latitude. To test this hypothesis, we compute the RCLV area fraction R_A (Fig. 9, bottom), which represents the average fraction of the ocean surface area that lies within an RCLV in each latitude band. For 30-day RCLVs, R_A peaks at around 0.025 and is an order of magnitude smaller for 90-day RCLVs. This is significantly higher than R_K , the diffusivity fraction, revealing that the RCLVs are actually regions of

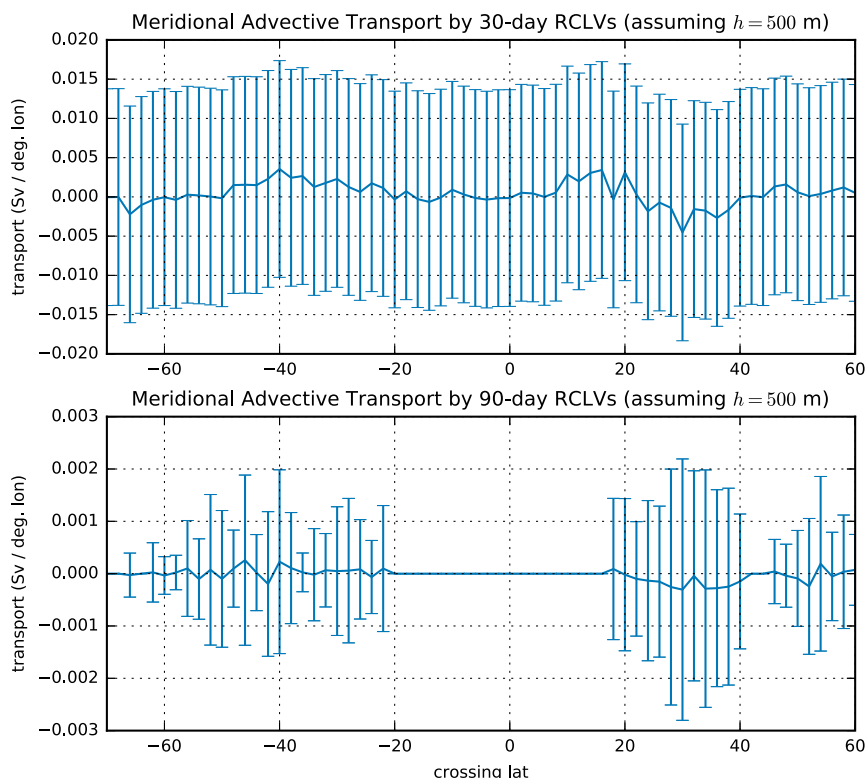


FIG. 8. Meridional advective transport latitude lines, calculated assuming a depth scale of 500 m. The error bar indicates one standard deviation of the time average over all time windows (30 days and 90 days).

anomalously *low* meridional dispersion. This is unsurprising, since the RCLVs remain coherent by construction and undergo relatively low filamentation compared to the background flow. In other words, randomly selected patches of ocean with the same surface area as the identified RCLVs would experience stronger meridional diffusion than the actual RCLVs.

6. Discussion and conclusions

Many prior studies have attempted to track mesoscale eddies by following anomalies in the SSH field (and associated instantaneous surface geostrophic velocity field) through time (e.g., CSS11; Dong et al. 2011; Faghmous et al. 2015). While such tracked Eulerian eddies may be useful for some applications, the work of Beron-Vera et al. (2013) and Haller and Beron-Vera (2013) has shown that structures identified in this way are not generally materially coherent: significant material leakage can occur through the supposed structure boundaries. This finding calls into question studies such as those of Dong et al. (2014) and Zhang et al. (2014), who attempt to infer heat, salt, and mass transports based on the displacement of tracked Eulerian eddies.

The goal of our study was to examine the material transport of mesoscale eddies defined as Lagrangian coherent structures.

We identified coherent eddies across a broad sector in the eastern Pacific using an objective, Lagrangian method based on the vorticity, the so-called RCLV approach of Haller et al. (2016). This computationally demanding task required the numerical advection of millions of virtual Lagrangian particles over a period of 25 years, the length of the satellite altimetry record. To our knowledge, our study is the largest-scale application of objective Lagrangian eddy detection to date. This comprehensive census of RCLVs in the sector allowed us to 1) calculate some statistical properties of RCLVs and 2) compute their contribution to net meridional transport via the coherent relative diffusivity $K_{\text{rel}}^{\text{cs}}$.

The occurrence frequency, length scales, and propagation speeds of RCLVs in this sector were found to be qualitatively similar to those of SSH eddies identified by CSS11. RCLVs were larger at low latitude, consistent with the meridional variations in the baroclinic Rossby deformation radius; the RCLV radii, however, were smaller than the SSH eddy radii by about a factor of 2. A more striking difference was the eddy lifetime; while we

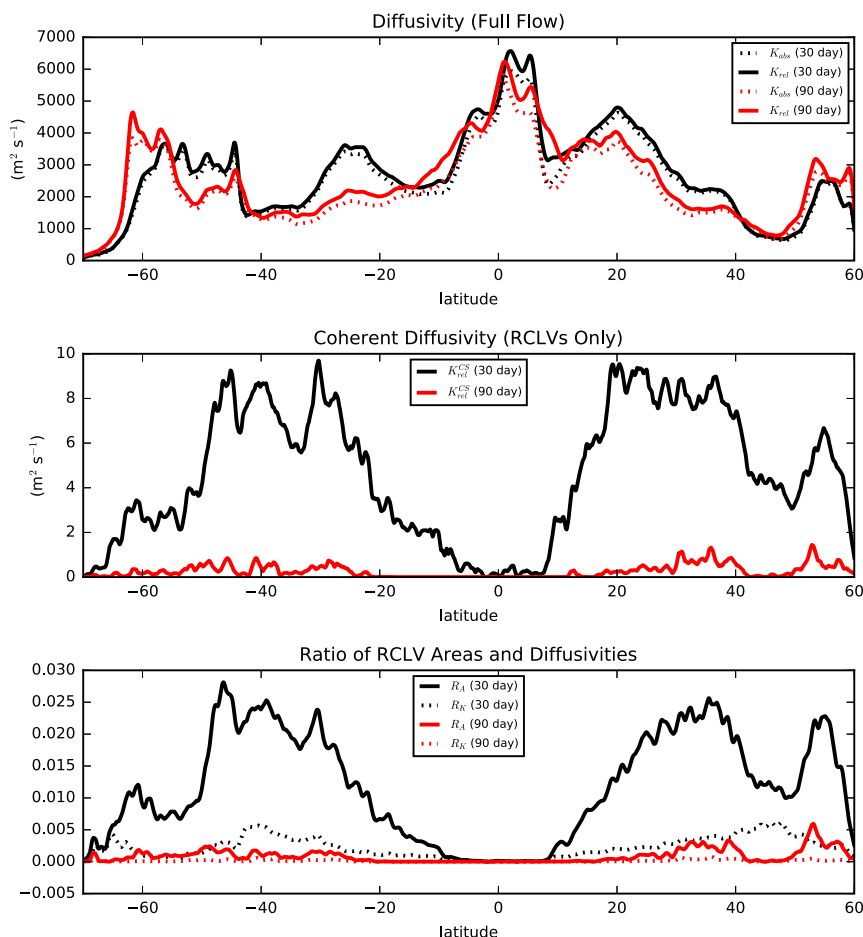


FIG. 9. (top) Full absolute (4) and relative diffusivity (5) averaged for all 30- (black) and 90-day (red) intervals. (middle) Coherent relative diffusivity (8) due only to the motion of RCLVs. Note the different scale on the y axis. (bottom) Nondimensional ratios of RCLV area (R_A) and diffusivity (R_K) to total area and diffusivity.

did not systematically examine the dependence on the extraction interval, we found essentially no RCLVs with lifetimes longer than 270 days. We suggested that this sets an upper bound on the leakiness time scale of mesoscale eddies in this sector. The comparison between RCLVs and SSH eddies raises many further questions about the relationship between the different methods. How often are RCLVs embedded inside SSH eddies? Is it possible to quantify the leakiness of the SSH eddies? Is the Eulerian nonlinearity parameter U/c (with U the azimuthal eddy velocity and c the translation speed) of CSS11 related to the presence of RCLVs? These questions are ripe for exploration in future work.

By assuming a fixed depth scale for our RCLVs, we calculated their advective volume transport and compared with the Eulerian PV-based estimate of Zhang et al. (2014). For 30-day RCLVs, we found similar spatial patterns to zonal and meridional advective volume transport, but lower by roughly one order of magnitude.

The 90-day RCLVs were rare enough that the associated transport estimates were somewhat noisy; however, they clearly showed even lower values of advective transport.

The primary focus and innovation of this paper is the definition and calculation of meridional diffusive transport by RCLVs. Since most climatically relevant gradients (temperature, salinity, nutrients, etc.) are strongest in latitude, meridional transport has the greatest relevance for the climate system. Our key finding is that $K_{\text{rel}}^{\text{CS}}$, representing the diffusive meridional transport due to RCLVs, is hundreds of times smaller than K_{rel} , the diffusive meridional transport of the full flow. This means that transport by RCLVs makes a negligible contribution to the net meridional dispersion. By a process of elimination, we can then conclude that, in this sector, meridional dispersion is primarily by incoherent motions, outside of the RCLV boundaries. This conclusion is in contradiction with the claims of Dong et al. (2014) regarding the role of coherent eddies in meridional heat

and salt transport. Our conclusion is, however, highly consistent with the findings of Wang et al. (2015), who used a different objective Lagrangian eddy identification method to quantify material transport by Agulhas rings. Indeed, Wang et al. (2015) found that the cross-Atlantic transport by materially coherent Agulhas eddies was two orders of magnitude smaller than prior estimates based on Eulerian eddy tracking. Since Agulhas rings move only in one direction, Wang et al. (2015) described the transport in terms of advection. In our sector, where eddies drift both north and south with equal frequency, transport was quantified in terms of diffusion. The overall conceptual agreement between their study and ours, which used a different method and examined a different region, suggests that relatively small material transport by coherent Lagrangian eddies is a robust result.

This finding does not mean, however, that coherent mesoscale eddies are insignificant for meridional transport. Indeed, studies in the spectral domain (e.g., Killworth et al. 2004; Abernathy and Wortham 2015) show that the eddy flux peaks at length scales and phase speeds associated with mesoscale eddies. Our results here, however, suggest that the meridional eddy transport is likely driven by stirring and filamentation on the periphery of coherent eddies, rather than by coherent meridional motion of the eddy core. This mechanism was illustrated clearly by Hausmann and Czaja (2012), who studied eddy heat transport by examining the cross-correlation structure between satellite-observed SSH and SST anomalies. Using the cross-correlation, they decomposed the Eulerian eddy heat flux into a drift component (associated with translation of fluid within the eddy core) and a swirl component, associated with peripheral stirring. They found that the swirl component was large enough to make a leading-order contribution to the oceanic heat budget, but that the drift component was negligible. This finding is compatible with our results, but not with Dong et al. (2014), who reached the opposite conclusion through methods similar to Hausmann and Czaja (2012).

A follow-up study by Y. Wang et al. (2016) challenges the notion of a binary division of the domain into *inside* and *outside* coherent eddies. That study examined a single Agulhas ring and documented a small, long-lived (2 years) vortex core embedded in a larger peripheral region with intermittently coherent boundaries continuously forming and decaying. The peripheral region was partly coherent but also exchanged fluid with the outside environment. Because some fluid was dragged along in the peripheral region as the eddy translated across the South Atlantic, Y. Wang et al. (2016) concluded that their earlier calculation (Wang et al. 2015) was potentially an underestimate of the material transport by Agulhas rings. Unfortunately, at this time there is

no objective method for identifying such peripheral semicoherent regions surrounding RCLV cores. We present our results as the transport due only to the strictly coherent rotational eddy core, acknowledging that, if such peripheral regions are commonplace, they would constitute an additional component of meridional transport.

Another limitation of the results we have presented is their reliance on the AVISO surface geostrophic velocities, which we have simply accepted at face value as adequately representative of the near-surface flow. In reality, there are many potential sources of error in these velocity fields, including measurement error of the altimeter itself, limited spatial and temporal sampling, mapping errors related to the gridding of satellite tracks, and the presence of ageostrophic and vertical velocities. LCSs represent stable attractors of the flow and are robust to the presence of small noise (Haller 2015). The spatial and temporal sampling issue, however, is likely more serious; Keating et al. (2012) showed that such subsampling can seriously degrade the finite-time Lyapunov exponent field in idealized turbulence simulations. It is an open question how the presence of submesoscale flows and internal waves impacts the leakiness of mesoscale transport barriers and eddies. A comprehensive investigation of the observational errors in the detection of LCSs from satellite altimetry observations would indeed be a valuable contribution. The full three-dimensional structure of RCLVs also remains an open question that is not possible to address using satellite observations alone. Analysis of a high-resolution general circulation model would be a good way to probe this question. Exploration of the prevalence of RCLVs, and their associated transport, in idealized models of baroclinic turbulence (e.g., the two-layer quasigeostrophic model; L. Wang et al. 2016) would also shed light on the relation of these structures to classical geophysical turbulence theory.

We see this study as the first step toward a fully global characterization of mesoscale coherent structures. It is our hope that this sort of detailed description of the Lagrangian kinematics of mesoscale transport will eventually lead to more accurate parameterization of mesoscale transport in coarse-resolution climate models. In the case of the eastern Pacific, it appears that we can reliably neglect long-range meridional transport due to fluid trapping within coherent eddy cores. This is good news from the perspective of parameterization, since the swirling mode of eddy transport seems more amenable to representation via diffusive closures. Determining whether such a conclusion holds more generally will have to await the completion of a global-scale Lagrangian eddy census, which is a serious computational challenge.

Acknowledgments. R.P.A. gratefully acknowledges the support of an NSF CAREER award (OCE 1553593). We thank Ci Zhang, Nathaniel Tarshish, Ivy Frenger, Carolina DuFour, and Steve Griffies for their feedback on this manuscript.

APPENDIX

Proofs of Objectivity

Here we show that (3)–(5) are objective with respect to a change in observer reference frame. We consider Euclidean observer changes of the form

$$\mathbf{x} = \mathbf{Q}(t)\mathbf{y} + \mathbf{b}(t), \quad (\text{A1})$$

where \mathbf{x} labels a point in the original frame, \mathbf{y} labels a point in the new frame, $\mathbf{Q}(t)$ is a proper orthogonal tensor [and hence $\mathbf{Q}^T(t)\mathbf{Q}(t) = \mathbf{I}$], and $\mathbf{b}(t)$ is a time-dependent translation vector; both $\mathbf{Q}(t)$ and $\mathbf{b}(t)$ are smooth functions of the time t .

We will work in a Euclidean space, as frame indifference with respect to (A1) is only meaningful in linear spaces. To reach a similar conclusion for objectivity on a curved surface (such as the Earth), one has to pull back the quantity of interest to (Euclidean) local coordinates, perform the observer change, and show objectivity in this coordinate space, then lift up the objectivity conclusions to the surface

via its local parameterization [cf. Haller et al. (2016) for a similar calculation].

a. Objectivity of meridional tracer flux

The instantaneous, pointwise Eulerian flux of a passive tracer $c(\mathbf{x}, t)$ under the velocity field $\mathbf{v}(\mathbf{x}, t)$ through a (possibly moving) straight line $\mathbf{x}_\ell(t; s)$ parameterized by the parameter s is, by definition,

$$\text{Flux}_{\mathbf{x}}[\mathbf{x}_\ell(t; s)] = c[\mathbf{x}_\ell(t; s), t] \left\{ \mathbf{v}[\mathbf{x}_\ell(t; s), t] - \frac{\partial}{\partial t} \mathbf{x}_\ell(t; s) \right\} \cdot \mathbf{n}_\ell(t; s), \quad (\text{A2})$$

where $\mathbf{n}_\ell(t; s)$ denotes the unit normal to line at time t , at the location $\mathbf{x}_\ell(t; s)$, and $\partial/\partial t[\mathbf{x}_\ell(t; s)]$ is the instantaneous velocity of the point $\mathbf{x}_\ell(t; s)$ of the straight line. Using (A1), the quantities $c[\mathbf{x}_\ell(t; s), t]$, $\mathbf{v}[\mathbf{x}_\ell(t; s), t]$, $\partial/\partial t[\mathbf{x}_\ell(t; s)]$, and $\mathbf{n}_\ell(t; s)$ involved in (A2) are linked to the counterparts $\hat{c}[\mathbf{y}_\ell(t; s), t]$, $\mathbf{w}[\mathbf{y}_\ell(t; s), t]$, $\partial/\partial t[\mathbf{y}_\ell(t; s)]$, and $\mathbf{m}(t; s)$ in the \mathbf{y} frame as follows:

$$c[\mathbf{x}_\ell(t; s), t] = c[\mathbf{Q}(t)\mathbf{y}_\ell(t; s) + \mathbf{b}(t), t] = \hat{c}[\mathbf{y}_\ell(t; s), t],$$

$$\mathbf{v}[\mathbf{x}_\ell(t; s), t] = \dot{\mathbf{Q}}(t)\mathbf{y}_\ell(t; s) + \mathbf{Q}(t)\mathbf{w}[\mathbf{y}_\ell(t; s), t] + \dot{\mathbf{b}}(t),$$

$$\frac{\partial}{\partial t} \mathbf{x}_\ell(t; s) = \dot{\mathbf{Q}}(t)\mathbf{y}_\ell(t; s) + \mathbf{Q}(t) \frac{\partial}{\partial t} \mathbf{y}_\ell(t; s) + \dot{\mathbf{b}}(t),$$

$$\mathbf{n}_\ell(t; s) = \mathbf{Q}(t)\mathbf{m}(t; s).$$

Substituting these relations into (A2) gives

$$\begin{aligned} \text{Flux}_{\mathbf{x}}[\mathbf{x}_\ell(t; s)] &= c[\mathbf{x}_\ell(t; s), t] \left\{ \mathbf{v}[\mathbf{x}_\ell(t; s), t] - \frac{\partial}{\partial t} \mathbf{x}_\ell(t; s) \right\} \cdot \mathbf{n}_\ell(t; s) \\ &= \hat{c}[\mathbf{y}_\ell(t; s), t] \left[\mathbf{Q}(t) \left\{ \mathbf{w}[\mathbf{y}_\ell(t; s), t] - \frac{\partial}{\partial t} \mathbf{y}_\ell(t; s) \right\} \right] \cdot \mathbf{Q}(t)\mathbf{m}(t; s) \\ &= \hat{c}[\mathbf{y}_\ell(t; s), t] \left\{ \mathbf{w}[\mathbf{y}_\ell(t; s), t] - \frac{\partial}{\partial t} \mathbf{y}_\ell(t; s) \right\}^T \mathbf{Q}^T(t)\mathbf{Q}(t)\mathbf{m}(t; s) \\ &= \hat{c}[\mathbf{y}_\ell(t; s), t] \left\{ \mathbf{w}[\mathbf{y}_\ell(t; s), t] - \frac{\partial}{\partial t} \mathbf{y}_\ell(t; s) \right\} \cdot \mathbf{m}(t; s) \\ &= \text{Flux}_{\mathbf{y}}[\mathbf{y}_\ell(t; s)], \end{aligned}$$

and hence the pointwise instantaneous Eulerian flux is objective. As a consequence, its average with respect to the parameter s along the line $\mathbf{x}_\ell(t; s)$ is also objective, and its subsequent average in time is also objective. In addition, linear lengths and time spans are constant under Euclidean observer changes, and hence

$$\frac{1}{T \cdot \text{length}(\mathbf{x}_\ell)} \int_{t_0}^{t_0+T} \int_s \text{Flux}_{\mathbf{x}}[\mathbf{x}_\ell(s)] ds dt$$

is also an objective quantity. But this last quantity is just a specific form of (1), with line $\mathbf{x}_\ell(t; s)$ being a steady zonal line $y = \text{const}$, and with the role of the parameter s played by x_0 .

b. Objectivity of K_{abs} in (3)

When (3) is taken as a definition of K_{abs} , then K_{abs} is necessarily objective, as the quotient of two objective quantities. If (4), by contrast, defined a nonobjective K_{abs} , then

Taylor's result would be incorrect, given that a nonobjective quantity cannot be identically equal to an objective quantity.

Let us therefore show that the coordinate-independent version of Taylor's (4) for K_{abs} is objective. Specifically, we need to show that the mean-squared Lagrangian distance of particles released at the same time t_0 from a (possibly moving) straight line $\mathbf{x}_0(t; s)$ of initial conditions is independent of the observer, which will imply the objectivity of K_{abs} as defined in (4) of the paper. This mean-squared Lagrangian distance, by definition, is

$$\overline{\text{dist}}_{\mathbf{x}}(t) = \int_s \{[\mathbf{x}(t; s) - \mathbf{x}_0(t; s)] \cdot \mathbf{n}_0(s; t)\}^2 ds, \quad (\text{A3})$$

$$\begin{aligned} [\mathbf{x}(t; s) - \mathbf{x}_0(t; s)] \cdot \mathbf{n}_0(t; s) &= \{\mathbf{Q}(t)[\mathbf{y}(t; s) - \mathbf{y}_0(t; s)]\} \cdot \mathbf{Q}(t)\mathbf{m}_0(t; s) \\ &= \{[\mathbf{y}(t; s) - \mathbf{y}_0(t; s)]\}^T \mathbf{Q}^T(t) \mathbf{Q}(t) \mathbf{m}_0(t; s) = \{[\mathbf{y}(t; s) - \mathbf{y}_0(t; s)]\} \cdot \mathbf{m}_0(t; s), \end{aligned} \quad (\text{A4})$$

and hence the integrand in (A3) is pointwise objective, rendering the full integral objective:

$$\overline{\text{dist}}_{\mathbf{x}}(t) = \overline{\text{dist}}_{\mathbf{y}}(t). \quad (\text{A5})$$

As noted above, this implies that K_{abs} in (4) is objective. Indeed, (A3) is just $(\Delta Y)^2$ in (4), when the initial condition line $\mathbf{x}_0(t_0; s)$ is specifically chosen to be $y_0 = 0$, parameterized via $s \equiv x_0$.

Most past studies have claimed that K_{abs} is not Galilean invariant (e.g., LaCasce 2008, their section 2). Since the Euclidean observer reference-frame changes represented in (A1) include Galilean transformations, our finding of objectivity contradicts a widely held view. In LaCasce (2008), it is claimed that ‘‘absolute dispersion is not Galilean invariant’’ because it reflects the particle drift from the starting location and is therefore influenced by the presence of a mean flow. However, advection by a mean flow is not equivalent to translation of the observer. Using our definition, all observers will measure the same absolute dispersion due to mean drift from the starting location. This objectivity is only achieved when distance is measured from the initial position as observed in the observer's current reference frame. Advection by a mean flow does not cause the initial position to move, but motion of the observer does. This subtle distinction explains the dichotomy between our definition and the conventional wisdom that K_{abs} is not objective.

c. Objectivity of K_{rel} in (5)

It is sufficient to show that the quantity, whose representation is $(Y - \bar{Y})^2$ in the frame of the Earth and in

where $\mathbf{x}(t; s)$ is the current position of the particle released from the point $\mathbf{x}_0(t_0; s)$ at time t_0 and $\mathbf{n}_0(t; s)$ is the normal along the line of initial conditions at time t . We stress that the observer needs to assess distances of particles at time t from the *currently observed* position of their release location. In the frame of the Earth, the release location does not move, and hence $\mathbf{x}_0(t; s) = \mathbf{x}_0(t_0; s)$ for all times. In a moving observer's frame, however, the observed release location $\mathbf{y}_0(t; s) = \mathbf{Q}^T(t)\mathbf{x}_0(t; s) = \mathbf{Q}^T(t)\mathbf{x}_0(t_0; s)$ does change with t . Focusing on the square root of the integrand in (A3) first, we use (A1) to note that

longitude–latitude coordinates, is objective. First we note that

$$\begin{aligned} (\Delta Y - \bar{\Delta Y})^2 &= [(\overline{Y - y_0}) - (\overline{Y - y_0})]^2 \\ &= [\overline{Y - \bar{Y} - (y_0 - \bar{y}_0)}]^2 = (\overline{Y - \bar{Y}})^2, \end{aligned} \quad (\text{A6})$$

since $\bar{y}_0 = y_0$ by definition. This quantity is the mean-squared deviation between the distance function of particles from their line of release and the mean of the same distance function. In other words, the quantity of interest is defined as

$$[\overline{\text{dist}}_{\mathbf{x}}(t) - \overline{\text{dist}}_{\mathbf{x}}(t)]^2 = \int_s \{[\mathbf{x}(t; s) - \mathbf{x}_0(t; s)] \cdot \mathbf{n}_0(s; t) - \overline{\text{dist}}_{\mathbf{x}}(t)\}^2 ds. \quad (\text{A7})$$

We have already concluded in (A4) that $[\mathbf{x}(t; s) - \mathbf{x}_0(t; s)] \cdot \mathbf{n}_0(s; t)$ is objective, and also in (A5) that $\overline{\text{dist}}_{\mathbf{x}}(t)$ is objective. As a consequence, the integrand of (A5) is pointwise objective, and hence (A5) itself is objective. This concludes the proof of objectivity of K_{rel} in (5).

REFERENCES

- Abernathey, R. P., and J. C. Marshall, 2013: Global surface eddy diffusivities derived from satellite altimetry. *J. Geophys. Res. Oceans*, **118**, 901–916, <https://doi.org/10.1002/jgrc.20066>.
- , and C. Wortham, 2015: Phase speed cross spectra of eddy heat fluxes in the Pacific. *J. Phys. Oceanogr.*, **45**, 1285–1301, <https://doi.org/10.1175/JPO-D-14-0160.1>.
- Adcroft, A., and Coauthors, 2018: MITgcm user manual. Massachusetts Institute of Technology Dept. of Earth, Atmospheric and Planetary Sciences Rep., 485 pp., http://mitgcm.org/public/r2_manual/latest/online_documents/manual.html.

- Bachman, S., and B. Fox-Kemper, 2013: Eddy parameterization challenge suite i: Eady spindown. *Ocean Modell.*, **64**, 12–18, <https://doi.org/10.1016/j.ocemod.2012.12.003>.
- Barnes, S. L., 1964: A technique for maximizing details in numerical weather map analysis. *J. Appl. Meteor.*, **3**, 396–409, [https://doi.org/10.1175/1520-0450\(1964\)003<0396:ATFMDI>2.0.CO;2](https://doi.org/10.1175/1520-0450(1964)003<0396:ATFMDI>2.0.CO;2).
- Batchelor, G., 1952: The effect of homogeneous turbulence on material lines and surfaces. *Proc. Roy. Soc. London*, **A213**, 349–366, <https://doi.org/10.1098/rspa.1952.0130>.
- Bennett, A. F., 1984: Relative dispersion: Local and nonlocal dynamics. *J. Atmos. Sci.*, **41**, 1881–1886, [https://doi.org/10.1175/1520-0469\(1984\)041<1881:RDLAND>2.0.CO;2](https://doi.org/10.1175/1520-0469(1984)041<1881:RDLAND>2.0.CO;2).
- Beron-Vera, F. J., Y. Wang, M. J. Olascoaga, G. J. Goni, and G. Haller, 2013: Objective detection of oceanic eddies and the Agulhas leakage. *J. Phys. Oceanogr.*, **43**, 1426–1438, <https://doi.org/10.1175/JPO-D-12-0171.1>.
- Chelton, D. B., R. A. de Szoeke, M. G. Schlax, K. Naggar, and N. Siwertz, 1998: Geographical variability of the first baroclinic Rossby radius of deformations. *J. Phys. Oceanogr.*, **28**, 433–450, [https://doi.org/10.1175/1520-0485\(1998\)028<0433:GVOTFB>2.0.CO;2](https://doi.org/10.1175/1520-0485(1998)028<0433:GVOTFB>2.0.CO;2).
- , M. G. Schlax, and R. M. Samelson, 2011: Global observations of nonlinear mesoscale eddies. *Prog. Oceanogr.*, **91**, 167–216, <https://doi.org/10.1016/j.pocean.2011.01.002>.
- Dong, C., F. Nencioli, Y. Liu, and J. C. McWilliams, 2011: An automated approach to detect oceanic eddies from satellite remotely sensed sea surface temperature data. *IEEE Geosci. Remote Sens. Lett.*, **8**, 1055–1059, <https://doi.org/10.1109/LGRS.2011.2155029>.
- , J. C. McWilliams, Y. Liu, and D. Chen, 2014: Global heat and salt transports by eddy movement. *Nat. Commun.*, **5**, 3294, <https://doi.org/10.1038/ncomms4294>.
- Ducet, N., P. Y. Le Traon, and G. Reverdin, 2000: Global high-resolution mapping of ocean circulation from TOPEX/Poseidon and ERS-1 and -2. *J. Geophys. Res.*, **105**, 19 477–19 498, <https://doi.org/10.1029/2000JC900063>.
- Faghmous, J. H., I. Frenger, Y. Yao, R. Warmka, A. Lindell, and V. Kumar, 2015: A daily global mesoscale ocean eddy dataset from satellite altimetry. *Sci. Data*, **2**, 150028, <https://doi.org/10.1038/sdata.2015.28>.
- Farazmand, M., and G. Haller, 2016: Polar rotation angle identifies elliptic islands in unsteady dynamical systems. *Physica D*, **315**, 1–12, <https://doi.org/10.1016/j.physd.2015.09.007>.
- Fox-Kemper, B., R. Lumpkin, and F. O. Bryan, 2013: Lateral transport in the ocean interior. *Ocean Circulation and Climate: A 21st Century Perspective*, G. Siedler et al., Eds., International Geophysics Series, Vol. 103, Elsevier, 185–209, <https://doi.org/10.1016/B978-0-12-391851-2.00008-8>.
- Gent, P., J. Willebrand, T. McDougal, and J. McWilliams, 1995: Parameterizing eddy-induced tracer transports in ocean circulation models. *J. Phys. Oceanogr.*, **25**, 463–475, [https://doi.org/10.1175/1520-0485\(1995\)025<0463:PEITTI>2.0.CO;2](https://doi.org/10.1175/1520-0485(1995)025<0463:PEITTI>2.0.CO;2).
- Haller, G., 2015: Lagrangian coherent structures. *Annu. Rev. Fluid Mech.*, **47**, 137–162, <https://doi.org/10.1146/annurev-fluid-010313-141322>.
- , 2016: Dynamic rotation and stretch tensors from a dynamic polar decomposition. *J. Mech. Phys. Solids*, **86**, 70–93, <https://doi.org/10.1016/j.jmps.2015.10.002>.
- , and F. J. Beron-Vera, 2012: Geodesic theory of transport barriers in two-dimensional flows. *Physica D*, **241**, 1680–1702, <https://doi.org/10.1016/j.physd.2012.06.012>.
- , and —, 2013: Coherent Lagrangian vortices: The black holes of turbulence. *J. Fluid Mech.*, **731**, R4, <https://doi.org/10.1017/jfm.2013.391>.
- , A. Hadjighasem, M. Farazmand, and F. Huhn, 2016: Defining coherent vortices objectively from the vorticity. *J. Fluid Mech.*, **795**, 136–173, <https://doi.org/10.1017/jfm.2016.151>.
- Hansen, A. E., D. Marteau, and P. Tabeling, 1998: Two-dimensional turbulence and dispersion in a freely decaying system. *Phys. Rev.*, **58E**, 7261, <https://doi.org/10.1103/PhysRevE.58.7261>.
- Hausmann, U., and A. Czaja, 2012: The observed signature of mesoscale eddies in sea surface temperature and the associated heat transport. *Deep-Sea Res. I*, **70**, 60–72, <https://doi.org/10.1016/j.dsr.2012.08.005>.
- Isern-Fontanet, J., E. García-Ladona, and J. Font, 2003: Identification of marine eddies from altimetric maps. *J. Atmos. Oceanic Technol.*, **20**, 772–778, [https://doi.org/10.1175/1520-0426\(2003\)20<772:IOMEFA>2.0.CO;2](https://doi.org/10.1175/1520-0426(2003)20<772:IOMEFA>2.0.CO;2).
- , J. Font, E. García-Ladona, M. Emelianov, C. Millot, and I. Taupier-Letage, 2004: Spatial structure of anticyclonic eddies in the Algerian Basin (Mediterranean Sea) analyzed using the Okubo–Weiss parameter. *Deep-Sea Res. II*, **51**, 3009–3028, <https://doi.org/10.1016/j.dsr2.2004.09.013>.
- Jayne, S. R., and J. Marotzke, 2002: The oceanic eddy heat transport. *J. Phys. Oceanogr.*, **32**, 3328–3345, [https://doi.org/10.1175/1520-0485\(2002\)032<3328:TOEHT>2.0.CO;2](https://doi.org/10.1175/1520-0485(2002)032<3328:TOEHT>2.0.CO;2).
- Keating, S. R., A. J. Majda, and K. S. Smith, 2012: New methods for estimating ocean eddy heat transport using satellite altimetry. *Mon. Wea. Rev.*, **140**, 1703–1722, <https://doi.org/10.1175/MWR-D-11-00145.1>.
- Killworth, P. D., P. Cipollini, B. M. Uz, and J. R. Blundell, 2004: Physical and biological mechanisms for planetary waves observed in satellite-derived chlorophyll. *J. Geophys. Res.*, **109**, C07002, <https://doi.org/10.1029/2003JC001768>.
- Klocker, A., and R. Abernathey, 2014: Global patterns of mesoscale eddy properties and diffusivities. *J. Phys. Oceanogr.*, **44**, 1030–1047, <https://doi.org/10.1175/JPO-D-13-0159.1>.
- , R. Ferrari, J. H. LaCasce, and S. T. Merrifield, 2012: Reconciling float-based and tracer-based estimates of eddy diffusivities. *J. Mar. Res.*, **70**, 569–602, <https://doi.org/10.1357/002224012805262743>.
- Kuijper, A., 2004: On detecting all saddle points in 2D images. *Pattern Recognit. Lett.*, **25**, 1665–1672, <https://doi.org/10.1016/j.patrec.2004.06.017>.
- LaCasce, J. H., 2008: Statistics from Lagrangian observations. *Prog. Oceanogr.*, **77**, 1–29, <https://doi.org/10.1016/j.pocean.2008.02.002>.
- Lagerloef, G., G. Mitchum, R. Lukas, and P. Niiler, 1999: Tropical Pacific near-surface currents estimated from altimeter, wind, and drifter data. *J. Geophys. Res.*, **104**, 23 313–23 326, <https://doi.org/10.1029/1999JC900197>.
- Morrow, R., J. Church, R. Coleman, D. Chelton, and N. White, 1992: Eddy momentum flux and its contribution to the Southern Ocean momentum balance. *Nature*, **357**, 482–485, <https://doi.org/10.1038/357482a0>.
- Okubo, A., 1970: Horizontal dispersion of floatable particles in the vicinity of velocity singularities such as convergences. *Deep-Sea Res. Oceanogr. Abstr.*, **17**, 445–454, [https://doi.org/10.1016/0011-7471\(70\)90059-8](https://doi.org/10.1016/0011-7471(70)90059-8).
- , 1971: Oceanic diffusion diagrams. *Deep-Sea Res. Oceanogr. Abstr.*, **18**, 789–802, [https://doi.org/10.1016/0011-7471\(71\)90046-5](https://doi.org/10.1016/0011-7471(71)90046-5).
- Ollitrault, M., C. Gabillet, and A. C. De Verdiere, 2005: Open ocean regimes of relative dispersion. *J. Fluid Mech.*, **533**, 381–407, <https://doi.org/10.1017/S0022112005004556>.
- Peacock, T., G. Froyland, and G. Haller, 2015: Introduction to focus issue: Objective detection of coherent structures. *Chaos*, **25**, 087201, <https://doi.org/10.1063/1.4928894>.
- Pierrehumbert, R. T., 1991: Chaotic mixing of a tracer and vorticity by modulated traveling Rossby waves. *Geophys. Astrophys. Fluid Dyn.*, **58**, 285–320, <https://doi.org/10.1080/03091929108227343>.

- Roemmich, D., and J. Gilson, 2001: Eddy transport of heat and thermocline waters in the North Pacific: A key to interannual/decadal climate variability? *J. Phys. Oceanogr.*, **31**, 675–687, [https://doi.org/10.1175/1520-0485\(2001\)031<0675:ETOHAT>2.0.CO;2](https://doi.org/10.1175/1520-0485(2001)031<0675:ETOHAT>2.0.CO;2).
- Rypina, I. I., I. Kamenkovich, P. Berloff, and L. Pratt, 2012: Eddy-induced particle dispersion in the near-surface Atlantic. *J. Phys. Oceanogr.*, **42**, 2206–2228, <https://doi.org/10.1175/JPO-D-11-0191.1>.
- Serra, M., and G. Haller, 2017: Efficient computation of null geodesics with applications to coherent vortex detection. *Proc. Roy. Soc. London*, **A473**, 20160807, <https://doi.org/10.1098/rspa.2016.0807>.
- Stammer, D., 1998: On eddy characteristics, eddy transports, and mean flow properties. *J. Phys. Oceanogr.*, **28**, 727–739, [https://doi.org/10.1175/1520-0485\(1998\)028<0727:OECETA>2.0.CO;2](https://doi.org/10.1175/1520-0485(1998)028<0727:OECETA>2.0.CO;2).
- Taylor, G. I., 1921: Diffusion by continuous movements. *Proc. London Math. Soc.*, **s2-20**, 196–212, <https://doi.org/10.1112/plms/s2-20.1.196>.
- Treguier, A. M., I. Held, and V. Larichev, 1997: Parameterization of quasigeostrophic eddies in primitive equation ocean models. *J. Phys. Oceanogr.*, **27**, 567–580, [https://doi.org/10.1175/1520-0485\(1997\)027<0567:POQEIP>2.0.CO;2](https://doi.org/10.1175/1520-0485(1997)027<0567:POQEIP>2.0.CO;2).
- Visbeck, M., J. Marshall, and T. Haine, 1997: Specification of eddy transfer coefficients in coarse-resolution ocean circulation models. *J. Phys. Oceanogr.*, **27**, 381–403, [https://doi.org/10.1175/1520-0485\(1997\)027<0381:SOETCI>2.0.CO;2](https://doi.org/10.1175/1520-0485(1997)027<0381:SOETCI>2.0.CO;2).
- Volkov, D., T. Lee, and L. Fu, 2008: Eddy-induced meridional heat transport in the ocean. *Geophys. Res. Lett.*, **35**, L20601, <https://doi.org/10.1029/2008GL035490>.
- Vollmer, L., and C. Eden, 2013: A global map of mesoscale eddy diffusivities based on linear stability analysis. *Ocean Modell.*, **72**, 198–209, <https://doi.org/10.1016/j.ocemod.2013.09.006>.
- Wang, L., M. F. Jansen, and R. P. Abernathy, 2016: Eddy phase speeds in a two-layer model of quasigeostrophic baroclinic turbulence with applications to ocean observations. *J. Phys. Oceanogr.*, **46**, 1963–1985, <https://doi.org/10.1175/JPO-D-15-0192.1>.
- Wang, Y., M. J. Olascoaga, and F. J. Beron-Vera, 2015: Coherent water transport across the South Atlantic. *Geophys. Res. Lett.*, **42**, 4072–4079, <https://doi.org/10.1002/2015GL064089>.
- , F. Beron-Vera, and M. Olascoaga, 2016: The life cycle of a coherent Lagrangian Agulhas ring. *J. Geophys. Res. Oceans*, **121**, 3944–3954, <https://doi.org/10.1002/2015JC011620>.
- Weiss, J., 1991: The dynamics of enstrophy transfer in two-dimensional hydrodynamics. *Physica D*, **48**, 273–294, [https://doi.org/10.1016/0167-2789\(91\)90088-Q](https://doi.org/10.1016/0167-2789(91)90088-Q).
- Wortham, C., and C. Wunsch, 2014: A multidimensional spectral description of ocean variability. *J. Phys. Oceanogr.*, **44**, 944–966, <https://doi.org/10.1175/JPO-D-13-0113.1>.
- Zhang, Z., W. Wang, and B. Qiu, 2014: Oceanic mass transport by mesoscale eddies. *Science*, **345**, 322–324, <https://doi.org/10.1126/science.1252418>.
- Zhurbas, V., and I. S. Oh, 2003: Lateral diffusivity and lagrangian scales in the Pacific Ocean as derived from drifter data. *J. Geophys. Res.*, **108**, 3141, <https://doi.org/10.1029/2002JC001596>.